High-Efficiency Plasma-Based Compressor for Ultrafast Soft X-Ray Free-Electron Lasers

Mingchang Wang[©], ^{1,2,*} Li Zeng, ^{3,*} Bingbing Zhang, ³ Qinghao Zhu, ³ Xiaozhe Shen, ³ Xiaofan Wang[©], ^{3,†} Qinming Li[©], ^{3,‡} and Weiqing Zhang[©]. ^{1,8}

¹Dalian Coherent Light Source and State Key Laboratory of Chemical Reaction Dynamics, Dalian Institute of Chemical Physics, Chinese Academy of Sciences, Dalian 116023, China

²University of Chinese Academy of Sciences, Beijing 100049, China
³Institute of Advanced Light Source Facilities, Shenzhen 518107, China

(Received 30 May 2025; accepted 16 September 2025; published 7 October 2025)

The generation of intense, femtosecond-scale x-ray pulses is crucial for probing matter under extreme

temporal and field conditions. Current chirped-pulse amplification (CPA) techniques in free-electron lasers (FELs), however, face efficiency limitations in the soft x-ray regime due to the inherent constraints of conventional optical compressors. To address this challenge, we propose a high-efficiency plasma-based compressor utilizing highly ionized noble gas plasma. Exploiting strong refractive index dispersion near ionic resonances, this scheme achieves over 70% transmission efficiency around 5.2 nm and is extendable to other highly charged ions for operation across the soft x-ray to vacuum ultraviolet range. Simulations demonstrate that a 25 fs FEL pulse can be compressed to 1.4 fs with peak power boosted to over 100 GW, while maintaining high-energy throughput. This transformative approach bridges the soft x-ray CPA gap and opens a scalable path toward compact, high-brightness attosecond FEL sources. DOI: 10.1103/d7r7-46ld

Free-electron lasers (FELs) operating in the attosecond-to-femtosecond regime, with their unprecedented temporal narrow intrinsic FEL bandwidth physically precludes the generation of few-femtosecond pulses. Advanced schemes, resolution and ultrahigh peak power, have revolutionized including chirped-pulse amplification (CPA) FELs [15,16]

the study of ultrafast dynamics in matter [1,2]. Soft x-ray ultrashort pulses, in particular, enable direct real-time

observation of electron transitions [3,4] and transient quantum phenomena [5], overcoming the temporal limitations of conventional spectroscopy. Furthermore, such high-power outputs are indispensable for applications requiring strong-field excitation [6] or quantum control [7], underscoring the critical role of intense ultrafast FELs in advancing attosecond science. To reach the femtosecond-to-attosecond regime, various approaches have been developed, such as emittance spoiling [8], low-charge operation [9], and so on [10–14]. However, these methods often reduce the effective charge participating in the amplification process, thereby limiting

the attainable pulse energy. This challenge is more fundamental in the soft x-ray and EUV regimes, where the *These authors contributed equally to this work. Contact author: wangxf@mail.iasf.ac.cn *Contact author: liqinming@mail.iasf.ac.cn §Contact author: weiqingzhang@dicp.ac.cn Published by the American Physical Society under the terms of the Creative Commons Attribution 4.0 International license. Further distribution of this work must maintain attribution to the author(s) and the published article's title, journal citation,

and DOI 0031-9007/25/135(15)/155001(6)

the entire electron bunch to contribute to emission.

A fundamental limitation in CPA-based FELs arises during the recompression stage. Conventional grating-based compressors suffer from limited efficiency in the soft x-ray regime, compounded by the need for precise alignment optics [15,18,19]. While multilayer mirrors and Bragg crystals provide partial mitigation within specific spectral

and techniques that counteract optical slippage [17], overcome both the temporal and energy limitations by simulta-

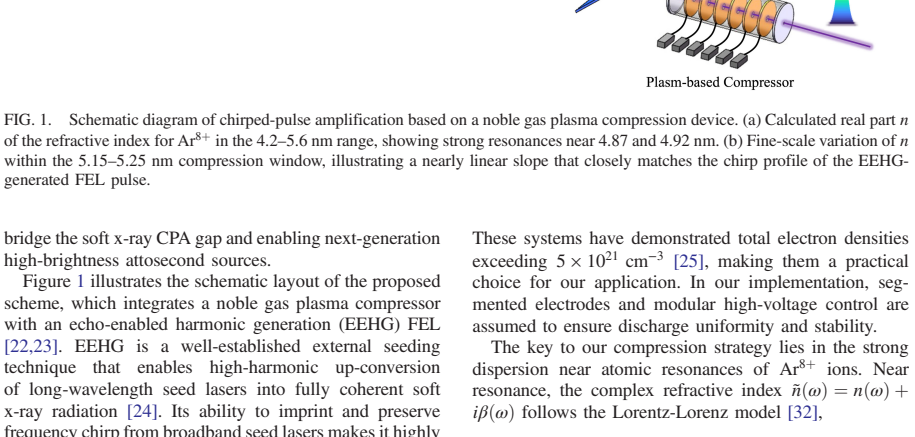
neously broadening the effective bandwidth while allowing

bands [16,20,21], a universal high-efficiency compression method remains elusive across the broad 1-10 nm regime. This bottleneck severely restricts the performance and scalability of soft x-ray CPA schemes.

To address this challenge, we propose a fundamentally different approach: a plasma-based compressor utilizing noble gas ions. By exploiting strong dispersion near resonant transitions in highly ionized atoms, this method offers broadband group velocity control and high transmission in the soft x-ray regime. Specifically, we demonstrate that a plasma column can compress a 25 fs FEL pulse to 1.4 fs with peak power exceeding 100 GW, while

maintaining a transmission efficiency of over 70%, a dramatic improvement over existing optical methods. Unlike conventional methods, this plasma compressor is scalable, tunable, and compatible with existing FEL infrastructures, offering a practical and transformative route to Published by the American Physical Society

155001-1 Chirp Compen (b)



frequency chirp from broadband seed lasers makes it highly $\frac{\tilde{n}^2 - 1}{\tilde{n}^2 + 2} = \frac{Ne^2}{3m_e \epsilon_0} \sum_j \frac{f_j}{\omega_{0j}^2 - \omega^2 - i\Gamma_j \omega}$ compatible with CPA strategies in soft x-ray FELs. In our configuration, two frequency-chirped seed lasers initiate (1)the EEHG process, imprinting chirp characteristics onto the high-harmonic microbunching and, subsequently, onto the FEL radiation. Specifically, we operate at the 53rd harmonic of the seed laser, generating soft x-ray pulses centered near 5.2 nm with a positive chirp inherited from where N is the ion density, f_j is the oscillator strength, and

nances enables efficient group-delay compensation. This two-stage approach, where EEHG enables coherent frequency multiplication and chirp preservation and the plasma compressor provides efficient pulse shortening, yields ultrafast high-power FEL output.

To ensure sufficient dispersion in the soft x-ray regime, we employ a 1-m-long plasma cavity filled with highly charged argon ions Ar^{8+} at a density of 2×10^{21} cm⁻³

This plasma is generated via a gas-puff Z-pinch discharge,

the seed. These chirped pulses are then directed into

plasma cavity, where strong dispersion near atomic reso-

which offers a compact and reproducible source of generating high-density noble gas plasma [25–27]. Compared to other plasma generation methods, such as electron cyclotron resonance [28], inertial confinement [29,30], and laser ablation [31], Z-pinch systems are well suited for generating extended volumes of highly charged ions.

0.6

0.4 0.2

FIG. 2. Absorption coefficient β (a) and transmission efficiency (b) near the Ar⁸⁺ resonance, both plotted over the 4.2–5.6 nm

To quantify the compressibility, the wave vector $k(\omega)$

 $n(\omega)\omega/c$ is expanded as a Taylor series. The second-order coefficient k_2 captures the group-delay dispersion (GDD),

wavelength range.

FEL pulses.

Figure 1(a) shows the calculated real part $n(\omega)$ of the refractive index for Ar⁸⁺ in the 4.2–5.6 nm range, based on this model and resonance data from the NIST database [33]. Two prominent peaks near 4.87 and 4.92 nm correspond to different fine-structure components of the $2s^22p^6 \rightarrow$ $2s^22p^53s$ transitions, and they induce strong anomalous dispersion and absorption. Focusing in on the working window, Fig. 1(b) highlights the behavior of *n* within 5.15–5.25 nm (shaded in rainbow).

In this region, the refractive index satisfies n > 1 with a negative slope-i.e., normal dispersion, where longer wave-

lengths travel faster than shorter ones. This trend is

essential for compensating the positive chirp of the FEL pulse. In contrast, the n < 1 region below resonance provides flat group velocity and fails to compress pulses effectively. Thus, selecting a bandwidth slightly above the

resonance ensures both effective dispersion and manage-

able absorption.

 ω_{0j} , Γ_j are the resonance frequency and width, respectively.

155001-2 PHYSICAL REVIEW LETTERS 135, 155001 (2025) temperatures, and high-charge-state ions (e.g.,

undergo resonance transitions at higher energies and do not absorb at 5.2 nm. Excited-state ions may contribute weak absorption, but their short lifetimes (hundreds of picoseconds to 10 ns) allow FEL pulses to pass once deexcitation occurs. To further ensure a clean medium, a transverse pulsed electric field can be applied to separate electrons from ions, suppressing reexcitation and extending plasma lifetime to tens of microseconds. It also spatially isolates ions of different charge states. When the laser beam is properly aligned with the Ar^{8+} region, a clean Ar^{8+} medium for chirp compensation is Supplemental Material, Secs. II–IV [34]). achieved To evaluate the performance of the proposed plasmabased compression scheme, we conducted comprehensive

numerical simulations using realistic parameters for a high-

gain seeded FEL. The simulations were performed with both GENESIS 1.3 [38] and OCELOT. The electron beam was configured with a central energy of 2.5 GeV, a relative slice energy spread of 8×10^{-5} , a normalized emittance of

0.5 mm mrad, and a peak current of 1.5 kA. The root-mean-square (rms) transverse beam size was approximately

 $35~\mu m$. A tailored energy chirp was applied to the electron

beam to locally match the frequency-chirped seed wavelength and maintain resonance along the radiator.

with an intrinsic spectral bandwidth of approximately 6.5%, enabling linear temporal stretching from a transform-limited duration of \sim 6.5–125 fs (FWHM). With a

waist size of approximately 0.5 mm and a peak power of

about 130 MW, these chirped pulses interacted with the electron beam in two modulators, each 2 m long with a 9 cm period length, imprinting energy modulation that faithfully inherited the seed chirp. The resulting dimensionless modulation amplitudes were approximately 5.8 for

The seed laser consisted of two pulses at 275.6 nm, each

both stages. The modulations were converted into highharmonic density structure via two dispersion sections with momentum compaction factors of 2.60 and 0.10 mm, respectively. The bunched beam subsequently entered a radiator composed of four 4-m-long undulators with 43 mm period length, tuned to 5.2 nm to generate and amplify chirped FEL pulses that matched the Ar⁸⁺ plasma reso-To characterize the temporal and spectral properties of the FEL pulses, we employed the Wigner distribution, which provides a joint time-frequency representation that simultaneously reveals the evolution of chirp and spectral structure. Figure 3(a) shows the Wigner distribution of the seed pulse, clearly revealing a linear chirp (high-frequency components lead, while low-frequency components lag) across a duration of 125 fs. At the radiator entrance, the

53rd-harmonic bunching factor [Fig. 3(b)] reaches a peak of ~5% with a temporal width of 46.7 fs (FWHM), notably

shorter than the seed pulse. This reflects an intrinsic feature of EEHG, wherein the microbunching length is inherently

Original Gaussian Fit After Compre Power [GW 60 Peak 40 20 Time [fs] FIG. 4. Temporal power profiles of FEL pulses before (blue) and after (red) plasma-based compression. preferential amplification of the central spectral components and an effectively shortened FEL pulse. The quasi-

periodic modulations in the uncompressed FEL pulse, arising from the interplay between the longitudinally

chirped bunching and the radiation slippage in the radiator,

are also a contributing factor to the side lobes that form

Nevertheless, the compression performance achieved

with a nontailored seed underscores the robustness and

generality of the proposed scheme. Further performance gains are anticipated through the introduction of a pre-

Such refinement would allow more precise phase matching

with the plasma dispersion and support near-transform limited pulse formation. Furthermore, the slight pulse shortening and observed modulations in Fig. 4 could be

compensating nonlinear chirp in the seed laser, feasible by the chirp-preserving nature of seeded FELs.

after compression. After passing through the plasma compressor, the FEL pulse is significantly shortened to 1.36 fs (FWHM), accompanied by an increase in peak power from 23.5 to 102.4 GW. The pulse energy decreases from 368 to 271 corresponding to a transmission efficiency of 73.6%. This value aligns well with the spectral transmission shown in Fig. 2(b), where the selected working window (5.15– $5.25\,$ nm) lies moderately above the Ar⁸⁺ resonance (4.92 nm), avoiding strong absorption while still providing sufficient dispersion. Notably, the reported pulse duration refers only to the main peak, excluding residual side lobes that originate from higher-order dispersion and carry a non-

to resonance, rather than absolute density. Accordingly, to achieve a comparable dispersion slope at lower density, the operating band must be shifted closer to the resonance (e.g., from 5.15-5.25 to 5.0-5.1 nm). Notably, transmission remains high within this shifted spectral window at reduced density, alleviating absorption concerns. Given that the seed laser chirp can be flexibly preadjusted in experiments, strong compression performance is thus attainable over a wide density range, confirming the scheme's feasibility This Letter proposed and validated a high-efficiency chirped-pulse compression scheme for soft x-ray free electron lasers, based on the resonance-enhanced dispersion of noble gas plasmas. By exploiting the strong frequency dependence of the real part of the refractive

extended across the soft x-ray to vacuum ultraviolet (VUV) spectral range (see Supplemental Material, Sec. V [34]). The proposed concept opens a scalable pathway to subfemtosecond, high-peak-power soft x-ray pulses, offering new opportunities for attosecond science, nonlinear x-ray optics, and photon-matter interaction studies in previously inaccessible regimes. Acknowledgments—We acknowledge the support of the staff members of Dalian Coherent Light Source [41]. We also sincerely thank Dr. Carlo Callegari and Dr. Kevin C. Prince of Elettra-Sincrotrone Trieste for their insightful discussions and valuable contributions to this work. This work is supported by the Scientific Instrument Developing Project of Chinese Academy of Sciences (Grant No. GJJSTD20220001), the National Natural Science Foundation of China (Grants No. 12305359, No. 22288201, and No. 22303055), the LiaoNing Talents Revitalization Program No. XLYC2202030), the Strategic Priority Research

[24] P. Rebernik Ribič, A. Abrami, L. Badano, M. Bossi, H.-H. Braun, N. Bruchon, F. Capotondi, D. Castronovo, M. Cautero, P. Cinquegrana et al., Nat. Photonics 13, 555 [25] R. Bleach, P. Burkhalter, D. Nagel, and R. Schneider, J. [25] K. Bieach, P. Burkhaiter, D. Nagei, and R. Schneider, J. Appl. Phys. 54, 1273 (1983).
[26] U. Shumlak, R. P. Golingo, B. A. Nelson, and D. J. Den Hartog, Phys. Rev. Lett. 87, 205005 (2001).
[27] S. A. Pikuz, D. B. Sinars, T. A. Shelkovenko, K. M. Chandler, D. A. Hammer, G. V. Ivanenkov, W. Stepniewski, and I. Y. Skobelev, Phys. Rev. Lett. 89, 035003 (2002). 035003 (2002). C. W. Chung, S. S. Kim, and H.-Y. Chang, Phys. Rev. Lett. 88, 095002 (2002). [29] S. H. Glenzer, B. MacGowan, P. Michel, N. Meezan, L. Suter, S. Dixit, J. Kline, G. Kyrala, D. Bradley, D. Callahan et al., Science 327, 1228 (2010). [30] R. Betti and O. Hurricane, Nat. Phys. 12, 435 (2016). [31] S. A. Irimiciuc, P.-E. Nica, M. Agop, and C. Focsa, Appl. Surf. Sci. 506, 144926 (2020).

electrons, other ionization states and excited states of ions, and the identification of resonance candidates across the soft

101201 (2016).

PHYSICAL REVIEW LETTERS 135, 155001 (2025)

Chirped X-ray FEL

Ultrafast FEL

which governs the main compression effect. For a linearly chirped input pulse described by $\omega(t) = \omega_0 + (a/\tau_0^2)t$, where a is a dimensionless coefficient indicating the strength of the longitudinal chirp and its relationship with GDD satisfies GDD = (τ_0^2/a) (see Supplemental Material, Sec. I [34]). Optimal compression occurs when the quadratic phase is precisely canceled by the plasma's dispersion. This happens under the condition $k_2 Z = \frac{\tau_0^2}{a}$ with Z = 1 m being the interaction length, yielding a transform-limited pulse duration τ_0 . The spectral slope of $n(\omega)$ in the selected window is closely matched to the frequency-time slope of the positively chirped FEL pulse generated via EEHG, enabling efficient plasma-based chirp

compensation and the production of high-power, ultrashort

Figure 2(a) presents the imaginary part β of the refractive

index, which governs absorption. Strong absorption occurs near the resonances at 4.87 and 4.92 nm, where β peaks and transmission approaches zero. In contrast, in the selected

5.15–5.25 nm region, β is significantly reduced. Figure 2(b) shows the corresponding transmission efficiency, calculated via the Beer-Lambert law,

Other plasma components, including free electrons, ions of various charge states, and excited-state ions, have negligible impact in this context. The plasma frequency

of free electrons lies in the UV range (~265 nm) and has no appreciable effect in the soft x-ray domain. Low-charge-state ions (e.g., Ar^{7+}) are suppressed at high electron

$$T=\exp\left(-\frac{4\pi\beta Z}{\lambda}\right). \tag{3}$$
 The transmission remains in the range of 60%–80%, making the plasma compressor both effective and practical for high-flux applications.

(2)

155001-3

PHYSICAL REVIEW LETTERS 135, 155001 (2025) Original 295 (a) (b) 0.04 Seed λ [nm

200

200

entrance of the radiator.

Time [fs]

5.24 (c)

5.20

ne [fs]

400

5.24 (d)

5.20

FEL \(\lambda\) [nm]

400

FIG. 3. Wigner distributions of the seed laser pulse (a) and FEL pulses before (c) and after (d) plasma-based compression. (b) Shows the bunching factor of the electron beam at the

reduced due to the localized phase space modulation, with

strict linearity, its local slope is broadly compatible with the

linear chirp of the seed laser, which was deliberately chosen

to represent a general, nontailored case. This partial

mismatch leads to residual phase distortions that hinder full energy convergence at the main peak, resulting in side lobes and limiting the effective peak power enhancement.

The temporal power profiles of the FEL pulse before and

after compression are shown in Fig. 4. According to standard CPA-free FEL pulse scaling, the expected pulse duration can be estimated as $\sigma_t^{\text{FEL}} \approx h^{-1} \sigma_t^{\text{seed}} \approx 33.27 \text{ fs}$

e [fs]

200

Time [fs]

400

higher harmonic orders yielding progressively narrower temporal structures [39]. The Wigner distribution of the FEL pulse prior to compression is shown in Fig. 3(c), demonstrating that the linear chirp is well preserved through the FEL amplification process. When propagating through the Ar^{8+} plasma, the position of each photon is updated as $s'=s+c\Delta t/n(\omega)$ for all spectral components, where c is the speed of light, and Δt is the traveling time. After propagation through the plasma cavity, the pulse undergoes substantial temporal compression [Fig. 3(d)]. This behavior arises from the anomalous group velocity dispersion near the plasma resonance: long-wavelength components at the pulse rear propagate faster negligible fraction of the energy. These features limit the peak power enhancement achievable under linear-chirp than short-wavelength components at the front, thereby enabling temporal overlap and compression. While the dispersion profile exhibits smooth curvature rather than seeding.

duration of 25.18 fs (FWHM). This discrepancy arises because the spectral bandwidth of the chirped bunching exceeds the gain bandwidth of the radiator, resulting in 280 万 **≅** 3.0 Peak Power [GW] -10 0 Plasma Density Deviation [%] FIG. 5. Impact of plasma density on pulse duration (blue), peak power (red), and pulse energy (yellow).

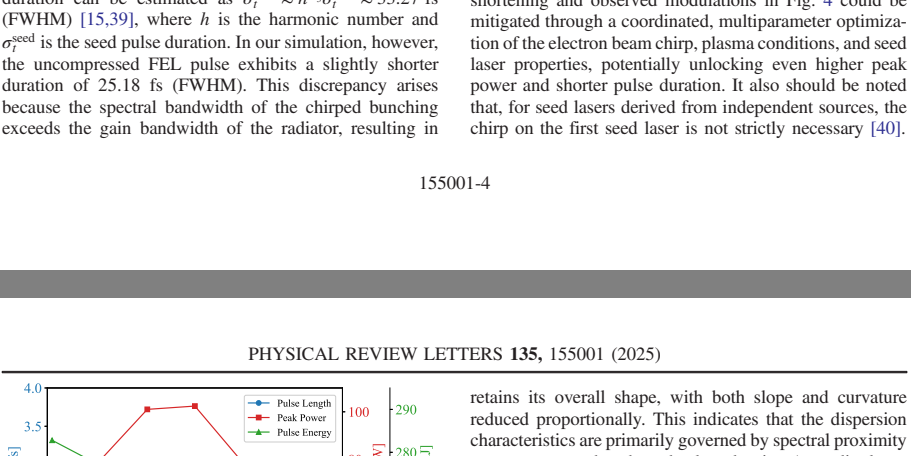
with respect to plasma density variations around the optimal value of $2 \times 10^{21} \, \mathrm{cm}^{-3}$. As shown in Fig. 5, deviations from this optimal density—whether positive or negative—inevitably shift the system away from the

these variations, the pulse duration remains below 3 fs across the entire $\pm 15\%$ density range, and the peak power stays above 48 GW. This divergence in trends highlights

the distinct physical mechanisms underlying temporal broadening and absorption and demonstrates the inherent resilience of the scheme under experimentally relevant

To evaluate the scheme's scalability, we extended the analysis to a more significant, tenfold reduction in plasma density, down to 2×10^{20} cm⁻³. The dispersion curve

plasma conditions.



ideal compression condition, resulting in longer pulse durations and lower peak powers. These two parameters exhibit a symmetric and monotonic trend: as the density increases or decreases, the pulse stretches and the peak power diminishes. In contrast, the pulse energy exhibits a distinctly different, asymmetric behavior. It peaks at the lowest plasma density, where absorption is minimal, and gradually decreases with increasing density due to stronger plasma absorption. Despite this, even at a +15% density deviation—where absorption is strongest—the output pulse energy remains as high as $259 \,\mu\text{J}$, corresponding to a transmission efficiency of 70.4%. Importantly, despite

014801 (2018). [13] P. K. Maroju, C. Grazioli, M. Di Fraia, M. Moioli, D. Ertel, H. Ahmadi, O. Plekan, P. Finetti, E. Allaria, L. Giannessi et al., Nature (London) 578, 386 (2020). [14] N. S. Mirian, M. Di Fraia, S. Spampinati, F. Sottocorona, E.

[1] P. Emma, R. Akre, J. Arthur, R. Bionta, C. Bostedt, J. Bozek, A. Brachmann, P. Bucksbaum, R. Decker *et al.*, Nat. Photonics **4**, 641 (2010). J. Duris, S. Li, T. Driver, E.G. Champenois, J.P. MacArthur, A.A. Lutman, Z. Zhang, P. Rosenberger, J. W. Aldrich, R. Coffee et al., Nat. Photonics 14, 30 (2020). T. Driver, M. Mountney, J. Wang, L. Ortmann, A. Al-Haddad, N. Berrah, C. Bostedt, E. G. Champenois, L. F. DiMauro, J. Duris et al., Nature (London) 632, 762 (2024).T. Driver, P. Rosenberger, E. G. Champe

(2005).[11] E. Prat and S. Reiche, Phys. Rev. Lett. 114, 244801 (2015).
[12] M. W. Guetg, A. A. Lutman, Y. Ding, T. J. Maxwell, F.-J. Decker, U. Bergmann, and Z. Huang, Phys. Rev. Lett. 120,

J. Zhu, Phys. Rev. Lett. 129, 213901 (2022).
 T. Tanaka, Phys. Rev. Lett. 114, 044801 (2015).
 M. Pascolini, S. Bonora, A. Giglia, N. Mahne, S. Nannarone, and L. Poletto, Appl. Opt. 45, 3253 (2006).
 F. Frassetto and L. Poletto, Appl. Opt. 54, 7985 (2015).
 Y. V. Shvyd'ko, M. Lerche, U. Kuetgens, H. D. Rüter, A. Alatas, and J. Zhao, Phys. Rev. Lett. 97, 235502 (2006).
 C. Bourassin-Bouchet, S. de Rossi, and F. Delmotte, in

index near ionic resonances, this method enables linear-chirp compensation with transmission efficiencies exceeding 70%. Numerical simulations demonstrate that a 25 fs FEL pulse can be compressed to approximately 1.4 fs, with the peak power enhanced beyond 100 GW, while preserv-

Program of the Chinese Academy of Sciences (Grant No. XDB0970000, subject No. XDB0970100), and the Shenzhen Science and Technology Program (Grant No. RCBS20221008093327057). Data availability—The data that support the findings of this article are openly available [42]. 155001-5

Surf. Sci. 506, 144926 (2020).
L. Drescher, O. Kornilov, T. Witting, G. Reitsma, N. Monserud, A. Rouzée, J. Mikosch, M. J. Vrakking, and B. Schütte, Nature (London) 564, 91 (2018).
A. Kramida, Y. Ralchenko, J. Reader, and N. A. Team, NIST

x-ray to VUV spectrum to demonstrate the generality and applicability of the proposed approach.

[35] D. Klir, A. V. Shishlov, V. A. Kokshenev, R. K. Cherdizov, J. Cikhardt, F. I. Fursov, J. Kravarik, P. Kubes, N. E. Kurmaev, J. Malir *et al.*, Phys. Plasmas **28**, 062708 (2021).[36] V. Tangri, A. J. Harvey-Thompson, J. L. Giuliani, J. W. Thornhill, A. L. Velikovich, J. P. Apruzese, N. D. Ouart, A. Dasgupta, B. Jones, and C. A. Jennings, Phys. Plasmas

Ferrari *et al.*, Nat. Commun. **7**, 13688 (2016) [16] H. Li, J. MacArthur, S. Littleton, M. Dunne, Z. D. Zhu, Phys. Rev. Lett. **129**, 213901 (2022). , Z. Huang, and

A. Al-Haddad, V. Averbukh, J. C. Barnard, N. Berrah, C. Bostedt et al., Science 375, 285 (2022).

[5] T. Barillot, O. Alexander, B. Cooper, T. Driver, D. Garratt, S. Li, A. Al Haddad, A. Sanchez-Gonzalez, M. Agåker, C. Arrell et al., Phys. Rev. X 11, 031048 (2021). [6] R. Boll, J. M. Schäfer, B. Richard, K. Fehre, G. Kastirke, Z. Jurek, M. S. Schöffler, M. M. Abdullah, N. Anders, T. M. Baumann et al., Nat. Phys. 18, 423 (2022).
[7] F. Richter, U. Saalmann, E. Allaria, M. Wollenhaupt, B. Ardini, A. Brynes, C. Callegari, G. Cerullo, M. Danailov, A. Demidovich *et al.*, Nature (London) **636**, 337 (2024). [8] Y. Ding, C. Behrens, R. Coffee, F.-J. Decker, P. Emma, C. Field, W. Helml, Z. Huang, P. Krejcik, J. Krzywinski et al., Field, W. Helml, Z. Huang, P. Krejcik, J. Krzywinski et al.,
Appl. Phys. Lett. 107, 191104 (2015).
[9] S. Huang, Y. Ding, Y. Feng, E. Hemsing, Z. Huang, J. Krzywinski, A. A. Lutman, A. Marinelli, T. J. Maxwell, and D. Zhu, Phys. Rev. Lett. 119, 154801 (2017).
[10] A. A. Zholents, Phys. Rev. ST Accel. Beams 8, 040701 (2005).

[37] J. B. Hasted, Proc. R. Soc. A 205, 421 (1951)

Allaria, L. Badano, M. B. Danailov, A. Demidovich, G. De Ninno, S. Di Mitri *et al.*, Nat. Photonics **15**, 523 (2021). [15] D. Gauthier, E. Allaria, M. Coreno, I. Cudin, H. Dacasa, M. B. Danailov, A. Demidovich, S. Di Mitri, B. Diviacco, E.

under less stringent plasma conditions. The transverse properties of the FEL pulse at saturation also satisfy practical requirements: the rms beam size is 101.9 $\,\mu m$ and the divergence is 16.0 $\,\mu rad$. These values fall well within the tolerances imposed by plasma uniformity and beamline apertures, ensuring that the transverse phase distortion remains minimal during propagation. Maintaining a compact transverse dimension is essential—not only to preserve compression fidelity by avoiding spatial inhomogeneity in ing more than 70% of the pulse energy. the plasma refractive index, but also to enable tighter plasma chamber apertures, which facilitate vacuum isolation and beamline integration. The simulated beam parameters validate This approach represents a transformative advancement in chirped-pulse amplification for FELs, overcoming the intrinsic efficiency limitations of grating-based compresthe practical feasibility of implementing this scheme in realistic experimental settings. sors in the soft x-ray regime. Moreover, by tailoring the plasma species and charge states, the scheme can be We further investigated the robustness of the scheme

PHYSICAL REVIEW LETTERS 135, 155001 (2025)

10.18434/T4W30F (2024). See Supplemental Material supplemental/10.1103/d7r7-46ld at http://link.aps.org/ which Refs. [33,35–37], for details about the theoretical model of chirped-pulse compression in dispersive media, the evaluation of the refractive index contribution from plasma

S. Reiche, Nucl. Instrum. Methods Phys. Res., Sect. A **429**, 243 (1999).

Alatas, and J. Zhao, Phys. Rev. Lett. 97, 253002 (2000).
[21] C. Bourassin-Bouchet, S. de Rossi, and F. Delmotte, in Optical Technologies for Extreme-Ultraviolet and Soft X-Ray Coherent Sources (Springer, New York, 2015), pp. 151–173.
[22] G. Stupakov, Phys. Rev. Lett. 102, 074801 (2009).
[23] D. Xiang and G. Stupakov, Phys. Rev. ST Accel. Beams 12, [41] https://cstr.cn/31127.02.DCLS. [42] 10.5281/zenodo.17141202. 030702 (2009)

[39] P. Finetti, H. Höppner, E. Allaria, C. Callegari, F. Capotondi, P. Cinquegrana, M. Coreno, R. Cucini, M. B.

Danailov, A. Demidovich, G. De Ninno, M. Di Fraia et al., Phys. Rev. X 7, 021043 (2017).

[40] N. S. Mirian, E. Allaria, N. Bruchon, P. Cinquegrana, M. B. Danailov, G. De Ninno, S. Di Mitri, E. Ferrari, L. Giannessi, E. Hemsing, G. Penco, E. Roussel, S. Spampinati, C. Spezzani, M. Trovó, M. Veronese, and P. Rebernik Ribič, Phys. Rev. Accel. Beams 23, 060701 (2020).

155001-6